ISBN 978-1-61284-167-0 - 978-90-75815-15-3

IEEE

Multilevel Converters for 10 MW Wind Turbines

Ke Ma
Frede Blaabjerg

Suggested Citation

K. Ma, F. Blaabjerg,"Multilevel Converters for 10 MW Wind Turbines," in Proc. of EPE' 2011, pp. 1-8, August 2011

Multilevel Converters for 10 MW Wind Turbines

Ke Ma, Frede Blaabjerg
Department of Energy Technology, Aalborg University
Pontoppidanstraede 101, Aalborg, Denmark
E-Mail: kema@et.aau.dk, fbl@et.aau.dk

Acknowledgements

The author would like to thank the funding support by China Scholarship Council.

Keywords

«Wind energy», «Multilevel converters», «Thermal stress».

Abstract

Several promising multi-level converter configurations for 10 MW Wind Turbines both with direct drive and one-stage gear box drive using Permanent Magnet Synchronous Generator (PMSG) are proposed, designed and compared. Reliability is a crucial indicator for large scale wind power converters, therefore the evaluations are mainly focused on the power device thermal performances, which are closely related to the life time and cost of the converter. Simulation results of different converter candidates regarding the loss and junction temperature are presented and analyzed. It is concluded that the three-level and five-level H-bridge converter topologies both have potential to achieve improved thermal performances compared to the three-level Neutral-Point-Clamped converter topology in the wind power application.

Introduction

The development of wind energy technologies has several significant trends in the past ten years [1]-[3],[5]: like size and capacity of the wind turbines grow rapidly, and making the price pr. produced kWh continuously reduced. The shortage of onshore land and booming need for renewable energy make newly established wind turbines moving from onshore to offshore wind farms. With stricter power grid integration requirements, the power electronics converters are changing from partial rated power to full rated power, and playing a more and more important role in the whole generation system. As the cutting-edge achievement, 7 MW offshore wind turbines with full rated power converter have already been shown on the market [3].

It is expected that 10 MW wind turbines will be the next longer-term target to be conquered according to the technology trends. Wind turbines at this power level are supposed to be located at large and remote offshore wind farms, where reliability issues need to be seriously taken into account because of significant impacts to the power grid and high cost for maintenance after a failure [4]. Up until now, there are still no final and dominant configurations on this power level, and questions still exist such as: the type and rotating speed of the generator, the topology and voltage levels/ratings of the converter as well as the availability and reliability, etc.

In this paper, several promising full-rated medium-voltage multi-level converters for 10 MW wind turbines are proposed, designed, and compared using PMSG. The evaluation criteria will mainly aim at the utilization and thermal performances of power switching devices. Simulation results regarding the loss and junction temperature distributions under different wind speeds are presented. With the information of junction temperature fluctuation and mean value, it is possible to further estimate the life time of each converter solution.

Possible configurations

As the interface between the wind turbines' generator and power grid, the wind power converter has to satisfy the requirements on the both sides, as summarized in Fig. 1.

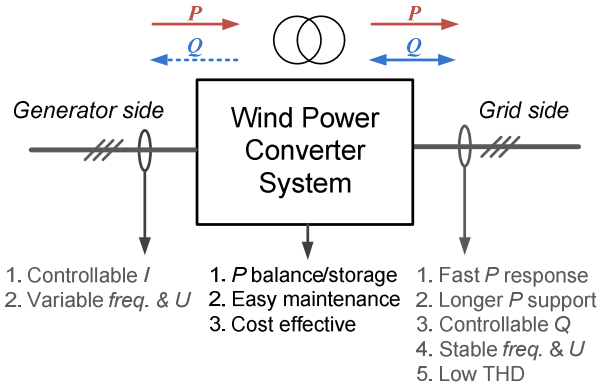

Fig. 1: Requirements for the modern wind power converter system. (*I* is the current, *U* is the voltage amplitude, *freq.* is the fundamental frequency, *P* is the active power, *Q* is the reactive power, and *THD* is the total harmonic distortion of current).

For the generator side: The current flowing in the generator's stator should be controlled to adjust the rotating speed. This will contribute to the active power balance during grid faults and help to extract the maximum power from the wind turbines [2]. Moreover, the converter should have the ability to handle variable fundamental frequency and voltage amplitude of the generator's output.

For the grid side: The converter must comply with the grid codes regardless of the wind speed. That means it should have the ability to control the injected/absorbed reactive power *Q*, and perform a fast active power *P* response. The fundamental frequency as well as voltage amplitude on the grid side should be almost fixed under normal operation, and the total harmonic distortion of the current must be maintained at a low level [5].

Inherently, the converter needs to satisfy both the generator side and grid side requirements with a cost effective and easy maintenance solution. That requires a high power density, reliability, modularity of the whole converter system. Moreover, the wind power converter may need the ability to store the energy, and boost up the voltage from generator side to the grid side.

According to the overall demands, four multilevel converter configurations for 10 MW wind turbines are proposed as follows [6]-[10], all of which can achieve the medium voltage rating.

3L-NPC BTB: As one of the most commercialized multilevel topologies on the market, three-level neutral point diode clamped converter is configured as a back-to-back structure, and shown in Fig. 2. The mid-point potential fluctuation of the DC bus is a main drawback, but this problem has been extensively researched and is considered improved [8]. However, it is found that the loss distribution between the outer and inner power devices in a switching arm is unequal, and this problem may lead to cost-ineffective power device utilization when it is practically designed [8], [9].

3L-HB BTB: This solution is composed of two three-phase H-bridge converters, as shown in Fig. 3. The clamped diodes in 3L-NPC solution are eliminated [10], and only half of the DC bus voltage is needed without mid-point, the cost for DC link capacitors can thereby be reduced. It is noted that an open winding structure in the generator will enable fault tolerant ability. However, extra length, cost, loss and inductance in the cables will be a major drawback. Also the zero-sequence current path is introduced in this configuration, special components or control methods are needed to block the zero-sequence current [10].

5L-HB BTB: This configuration is composed of two back-to-back H-bridge converters making use of 3L-NPC switching arms, as shown in Fig. 4. It is an extension of 3L-HB BTB, and shares the same special requirements for open-winding generator and transformer. With switching devices of the same voltage rating, 5L-HB BTB can achieve five-level output voltage and doubled voltage amplitude compared to the 3L-NPC and 3L-HB solution. These features enable less current rating of the

switching devices as well as the cables [10], [11]. However, the 5L-HB BTB introduces more power devices, which could increase the cost, and has the drawback of unequal loss distribution of power devices like the 3L-NPC BTB.

3L-NPC+5L-HB: This "compound" configuration employs 3L-NPC topology on the generator side, and 5L-HB on the grid side, as shown in Fig. 5. The voltage levels and amplitude of the grid side is higher than those on the generator side.

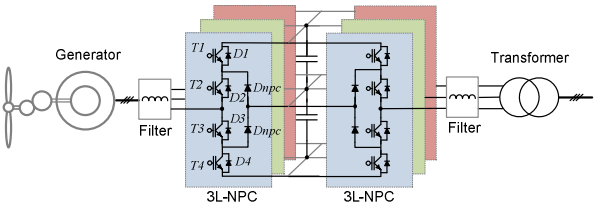

Fig. 2. Three-level Neutral Point Clamped back-to-back configuration. (***3L-NPC BTB***).

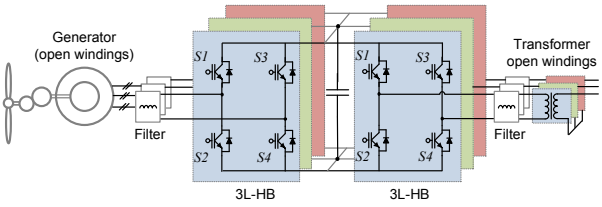

Fig. 3. Three-level H-bridge back-to-back configuration. (***3L-HB BTB***).

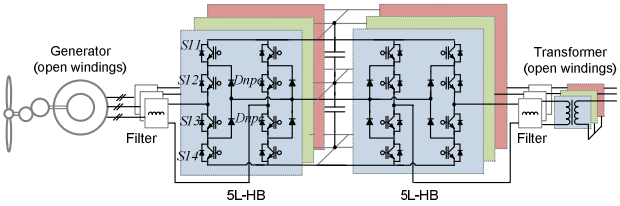

Fig. 4. Five-level H-bridge back-to-back configuration. (***5L-HB BTB***).

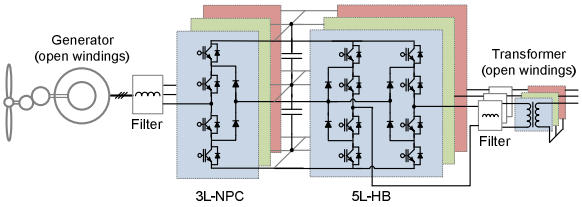

Fig. 5. "Compound" configuration. (***3L-NPC + 5L-HB***).

Basic design criteria

In order to conduct evaluation of each converter candidate, the parameters of generator and basic design for converters are needed. The parameters of 10 MW PMSG with one-stage gear box (PMSG_1G) and direct (PMSG_DD) drive are shown in Table I, which is acquired from [12] and [13]. The gear box ratio R for PMSG_1G is designed at 9.7 (which results in 120 Hz rated electrical frequency) to achieve an optimal tradeoff between the cost of generator and gear box as claimed in [12].

Table I: Parameters for 10 MW PMSG [12], [13]

Generator type	**PMSG_DD**	**PMSG_1G**
Rated wind speed v_w (m/s)	11.7	
Rated rotor speed n_r (rpm)	10	
Air gap diameter D (m)	10	4.2
Stator length l (m)	1.8	0.9
Number of pole pairs N_p	165	74
Gear box ratio R	-	9.7
Rated shaft speed n_s (rpm)	10	97
Rated electrical frequency f_e (Hz)	27.5	120
No load induced voltage E_p (Vrms)	3748 / 1874	3600 / 1800
Synchronous inductance L_s (mH)	11 / 2.76	3.16 / 0.79

Regarding the parameters of the converter, all of the power switching devices have the commutated voltage at 2.8 kV in order to utilize the available and dominant 4.5 kV high-power IGCT/IGBT on the market. For simplicity of analysis, the power grid is considered as three 20 kV/50 Hz ideal AC voltage sources, the resistance in the generator and the cables is not taken into account, DC bus capacitance is assumed high, and the transformers are assumed ideal.

Design of grid side converters

According to the commutated voltage of power devices (2.8 kV), the DC bus and maximum output voltage of each configuration can be determined. The equivalent switching frequency f_s of the grid side converter is designed at 800 Hz in order to get an acceptable switching loss of the power devices. The output filter inductance is designed to limit the maximum current ripple to 25% of the rated maximum current amplitude, and the filter capacitance is not taken into account. The power control method of the converter can be found in [4].

Design of generator side converters

The equivalent switching frequency of the generator side converter is designed as 10 times of the generator's maximum fundamental frequency f_e. For simplicity, filters on the generator side are not considered. Constant stator voltage control is used when the wind speed is above 11 m/s, and the maximum torque control is used when the wind speed is below 11 m/s [12]. Because there is a zero-sequence-current path, the third harmonic injection modulation method cannot be applied in the generator side converter with 3L-HB and 5L-HB topologies [10]. The detail parameters of the grid side and generator side converter in each solution are summarized in Table II and Table III respectively. The parameters for the DC bus voltage, component numbers and modulation method are summarized in Table IV.

Table II: The parameters for grid side converters

Grid side converter PF_g=0.9, P_{rated}=10 MW, f_s=800Hz				
Configurations	**3L-NPC**	**3L-HB**	**5L-HB**	**3L +5L**
Apparent power	13.38 MW	13.38 MW	12.45 MW	12.45 MW
Rated output voltage[1]	3970 V	3970 V	7400 V	7400 V
Primary side voltage[2]	3300 V	3300 V	6600 V	6600 V
Rated current	1944 A	1944 A	972 A	972 A
Filter inductance	1.13 mH	1.13 mH	2.89 mH	2.89 mH
Transformer[3]	Y/Y	O/Y	O/Y	O/Y
Fault tolerant ability	No			

Table III: The parameters for generator side converters

Generator side converter (PMSG_DD/PMSG_1G)				
Configurations	**3L-NPC**	**3L-HB**	**5L-HB**	**3L + 5L**
Apparent power	10.36 / 10.84 MW			
Rated stator voltage	3300 V	3300 V	6600 V	3300 V
Induced voltage[4]	3246/3118 V	3246/3118 V	6491/6237 V	3246/3118 V
Rated current	1813/1897 A	1813/1897 A	906/948 A	1813/1897 A
Stator inductance	2.76/0.79 mH	2.76/0.79 mH	11/3.16 mH	2.76/0.79 mH
Equivalent sw. freq.	275/1200 Hz			
Fault tolerant ability	No	Yes	Yes	No

Note:
1. line-to-line fundamental voltage before filter inductor. 2. Line-to-line voltage on the primary windings of transformer.
3. O means open winding connection. 4. Induced line-to-line voltage in the generator.

Table IV: The DC bus, components and modulation strategy

Configurations	**3L-NPC**	**3L-HB**	**5L-HB**	**3L +5L**
DC bus voltage	5.6 kV	2.8 kV	5.6 kV	5.6 kV
IGBT number	24	24	48	36
Diode number*	36	24	72	54
PWM methods	PD-PWM	Unipo-PWM	POD-PWM	PD-PWM +POD-PWM

* Include neutral point clamping diodes and anti-parallel freewheeling diodes.

Loss distribution

The loss model shares the same idea in [14],[15], which is a commonly accepted method for the loss evaluation of power semiconductor devices, and the loss simulation is carried out based on PLECS Blockset in Simulink [16]. Press-pack IGCT 5SHY35L4512 (commutated voltage 2.8 kV/ maximum current 3.3 kArms) and diodes 5SDF16L4503 (2.8 kV/2.6 kArms) from ABB are chosen as the switching power devices for 3L-NPC and 3L-HB topologies. IGCT 5SHY35L4510 (2.8 kV/2.7 kArms) and diodes 5SDF10H4503 (2.8 kV/1.8 kArms) from ABB are chosen for the 5L-HB topology. Losses in the reactive components are not considered in this paper.

The loss distribution of the grid side and generator side converters (with both direct-drive and one-stage gear box drive PMSG) are illustrated in Fig. 6, Fig. 7 and Fig. 8, in which the loss in each power device of a switching arm is indicated. 3L-NPC+5L-HB configuration is not shown because it shares the same performances with the generator side converter in 3L-NPC BTB as well as the grid side

converter in 5L-HB BTB respectively. It can be seen that the loss distribution characteristics are quite different not only between the configurations, but also between the generator side and grid side.

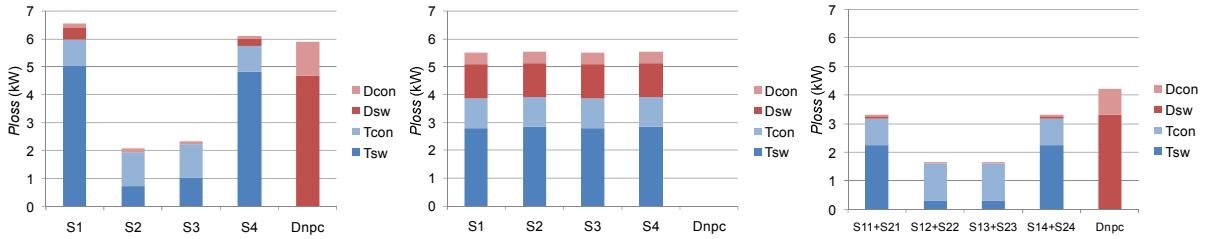

(a) 3L-NPC BTB (b) 3L-HB BTB (c) 5L-HB BTB

Fig. 6: Loss distribution of grid side converter solutions (P_G=10MW). Dcon and Dsw are the conduction and switching loss in diodes respectively, Tcon and Tsw are the conduction and switching loss in the IGCT respectively. Dnpc includes all NPC diodes in a switching arm.

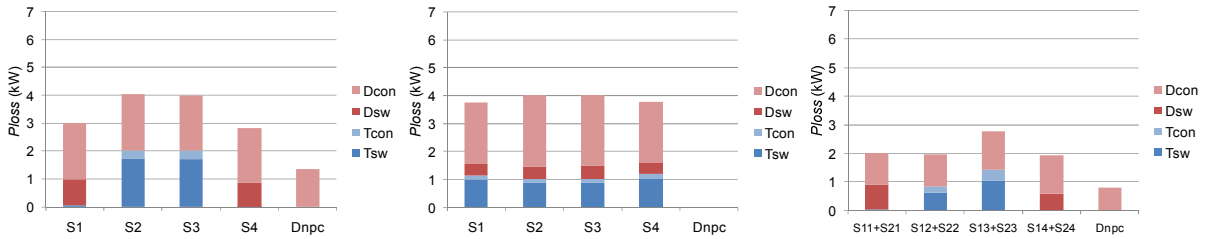

(a) 3L-NPC BTB (b) 3L-HB BTB (c) 5L-HB BTB

Fig. 7: Loss distribution of generator side converter solutions with direct-drive PMSG (P_G=10MW).

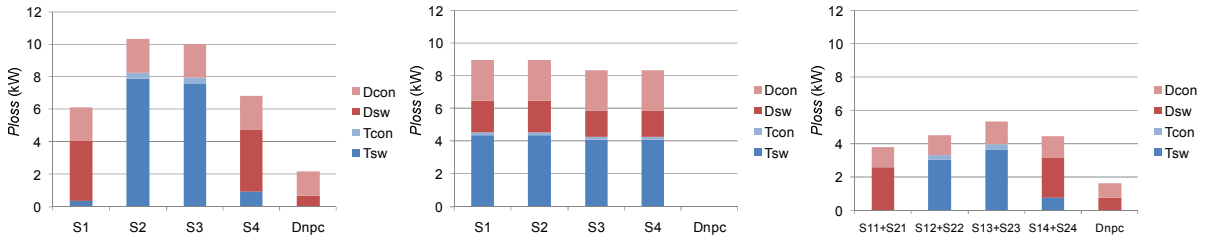

(a) 3L-NPC BTB (b) 3L-HB BTB (c) 5L-HB BTB

Fig. 8: Loss distribution of generator side converter solutions with one-stage gear box drive PMSG (P_G=10MW).

For the grid side converter, the IGCTs and clamped diodes dissipate significantly more loss than the freewheeling diodes in all of the candidate topologies. 3L-NPC BTB shows dramatically unequal loss distribution between outer switches and inner switches. While the loss distribution of 3L-HB BTB configuration is much more equal. The 5L-HB BTB shares similar unequal loss distribution with 3L-NPC BTB, but the loss distribution inequality is not so serious because of half current rating and less switching losses in power devices.

For the generator side converter with direct-drive PMSG, the diodes dissipate significantly more loss than the IGCTs, and conduction loss is dominant in the diodes. The unequal loss distributions in 3L-NPC and 5L-HB topologies are improved, and the loss dissipated in the clamped diodes is much less than that in the grid side converters because of eliminated switching loss.

For the generator side converter with one-stage gear box PMSG, the switching loss both in the IGCTs and diodes increase significantly in all of the candidate topologies. The 3L-HB BTB shows a perfect equal loss distribution not only between switches but also between IGCTs and diodes.

Thermal distribution

The thermal performances of power devices are closely related to the reliability of converter, current rating of power devices and cost of the cooling system, therefore it is an important indicator for large scale wind power converters. In order to conduct thermal performances evaluation, an appropriate thermal model should be first acquired.

Thermal model

The thermal models of a single switch and clamped diode are indicated in Fig. 9 [15],[19], in which the thermal impedance from junction to case $Z_{(j\text{-}c)}$ is modeled as a four-layers Foster RC network, as shown in Fig. 10. Each of the thermal parameters can be found from the manufacturer datasheets and they are summarized in Table V, where the thermal resistance R_{th} will decide the steady state mean value of junction temperature, and the thermal capacitance (with time constant τ) will decide the dynamic change or fluctuation of the junction temperature. The ambient temperature is set to 50 ℃ and considered constant during the operation of converter.

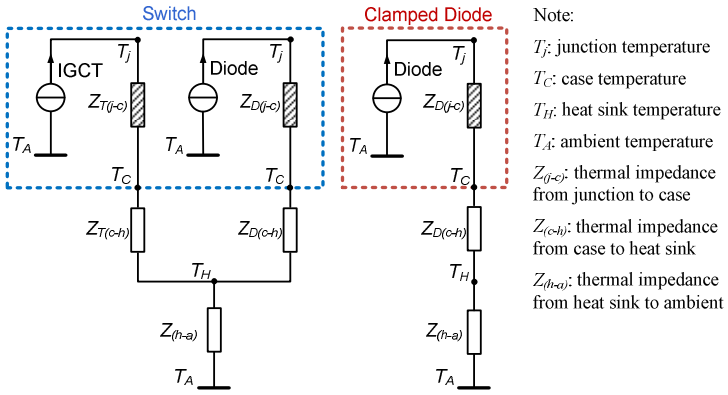

Fig. 9: Thermal models of the power devices

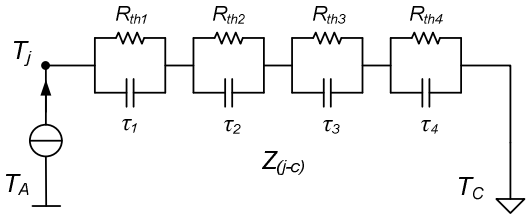

Fig. 10: Thermal model of the impedance $Z_{T(j\text{-}c)}$ and $Z_{D(j\text{-}c)}$ from junction to case in Fig. 9

Table V: Parameters of thermal impedance for IGCT/diode

Thermal Impedance	$Z_{(j\text{-}c)}$				$Z_{(c\text{-}h)}$
	Sector 1	**Sector 2**	**Sector 3**	**Sector 4**	
R_{iIGCT} (K/kW)	5.562	1.527	0.868	0.545	3
τ_{iIGCT} (s)	0.5119	0.896	0.0091	0.0024	-
R_{iDiode} (K/kW)	11.124	3.054	1.736	1.09	6
τ_{iDiode} (s)	0.5119	0.896	0.0091	0.0024	-

It is noted that the separately packaged IGCT and diodes are chosen because of the limitation for available products which can be found on the market. However, in a practical converter design, the IGCT/IGBT and its freewheeling diode are usually integrated and packaged together, the chip size for diode is usually about half of that for the IGCT/IGBT, accordingly, the thermal resistance of the diode from junction to heat sink is not consistent with its datasheet but set to twice of the IGCT.

Normally, the thermal capacitance outside a power device from case to ambient are much larger compared to that inside a power device from junction to case in a properly designed cooling system. The larger thermal capacitance, which has longer time constant ranging from hundreds of milliseconds to hundreds of seconds [19], mostly decide the time to achieve steady-state junction temperature, and have no significant impacts on the dynamic junction temperature fluctuation within a fundamental cycle of the converter output (dozens of milliseconds). Therefore it is efficient to make a simplification which ignores the relative larger thermal capacitances in $Z_{(c\text{-}h)}$ and $Z_{(h\text{-}a)}$ to realize a faster thermal simulation. In mega-watts power converter systems, separated heat sink is typically used, a good thermal decoupling among the power devices can be achieved, so the thermal resistance between heat sink and ambient is considered small.

Based on the previous loss simulation results and thermal model, the junction temperature of power devices in each of the converter solution can be simulated with the PLECS blockset in Simulink [16].

Thermal performance of grid side converters

The thermal performances of a converter mainly consist of three aspects of the junction temperature in the power switching devices: the distribution equality (which is related to the efficiency of device utilization), mean value (which is related to the maximum achieved junction temperature) as well as

the fluctuation amplitude (which is related to the life time), the evaluation of thermal performances will be based on the three aspects. The simulation results of power device junction temperatures in each of the grid side converter candidate are shown in Fig. 11, in which the converters are operating under rated and steady-state condition, and the simulation time of 10 output fundamental cycles (0.2 s) are illustrated. It can be seen that the three aspects of thermal performances are quite different among topologies and power devices.

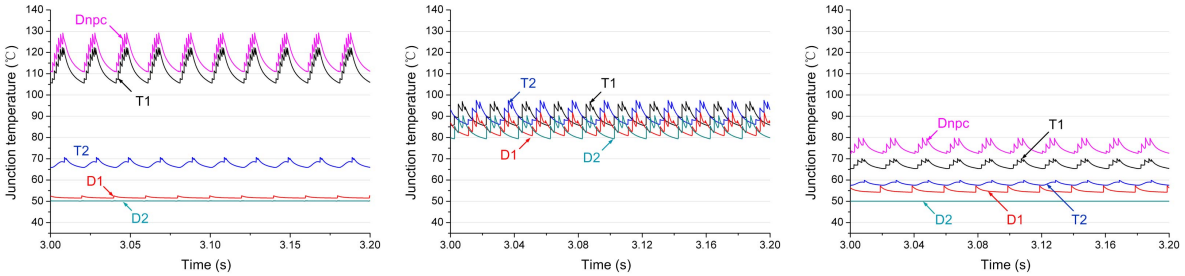

(a) 3L-NPC BTB (b) 3L-HB BTB (c) 5L-HB BTB

Fig. 11: Thermal distribution of grid side converters (v_w=11.7 m/s, P_G=10 MW, f_g=50Hz).

For the 3L-NPC converter, as shown in Fig. 11 (a), the temperature distribution is quite unequal, this is consistent with the loss simulation results in Fig. 6 (a). The clamped diode Dnpc and outer IGCT T1 are the hottest devices with much higher junction temperature mean value and fluctuation amplitude compared to other power devices. While the 3L-HB converter shows a perfect equal temperature distribution and has 35 ℃ lower maximum junction temperature compared to the 3L-NPC, as shown in Fig. 11 (b). For the 5L-HB converter, as shown in Fig. 11 (c), the equality of thermal distribution is better than 3L-NPC but worse than 3L-HB converter. However, it achieves the lowest overall junction temperature, and has the most potential to further reduce the current rating and cost of power devices.

The further comparison of junction temperature fluctuation ΔT_j and mean value T_m with relation to the wind speed v_w between different grid side converters are shown in Fig. 12 and Fig. 13 respectively, where the most extreme loaded power devices in each converter solution are indicated. The parameters for the grid side converter at different wind speeds are summarized in Table VI. It can be seen that, 3L-NPC shows both the largest ΔT_j as well as T_m during nearly the whole operation range of wind speeds. The 3L-HB reduces ΔT_j and T_m by 7 ℃ and 30 ℃ under rated wind speed 11.7 m/s. The 5L-HB can further reduce the ΔT_j and T_m compared to 3L-HB topology but the improvement is not significant. As a result, 3L-HB topology shows an appropriate tradeoff between the thermal performances and cost of components, and thereby is attractive as the grid side converter.

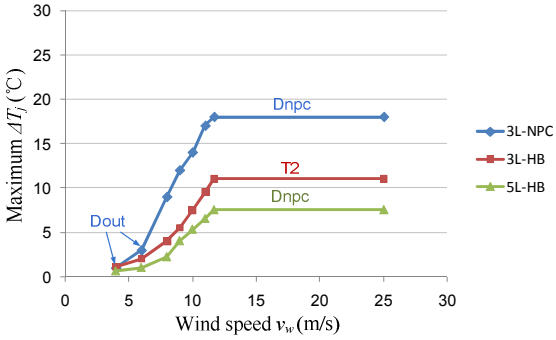

Fig. 12: Temperature fluctuation ΔT_j vs. wind speed v_w of grid side converters

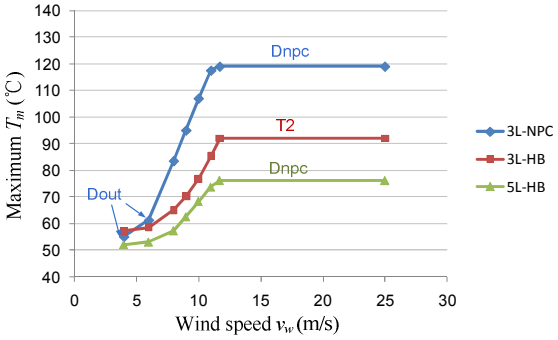

Fig. 13: Temperature mean value T_m vs. wind speed v_w of grid side converters

Table VI: The parameters of grid side converter at different wind speeds

Wind speed v_w (m/s)	**4**	**6**	**8**	**9**	**10**	**11**
Generator power P_G (MW)	0.4	1.4	3.2	4.6	6.3	8.4
Primary side voltage (Vrms)*	1908/3815					
Fundamental frequency f_g (Hz)	50					
Switching frequency f_s (Hz)	800					

*Phase voltage in the primary windings of transformer.

Thermal performance of generator side converters

The simulation results of junction temperatures in each of the generator side converter both with direct-drive PMSG (PMSG_DD) and one-stage gear box drive PMSG (PMSG_1G) are shown in Fig. 14 and Fig. 15 respectively, in which the converters are operating under rated and steady-state condition, and the same simulation time (0.2 s) as grid side converter are illustrated. It can be seen that, the converters with PMSG_1G have more frequent temperature fluctuation compared to those with PMSG_DD, but the fluctuation amplitude and trends of distribution equality are similar in the two drive systems. The temperature mean values in the converters with PMSG_1G are higher than those with PMSG_DD because of much higher switching loss as simulated in Fig. 8.

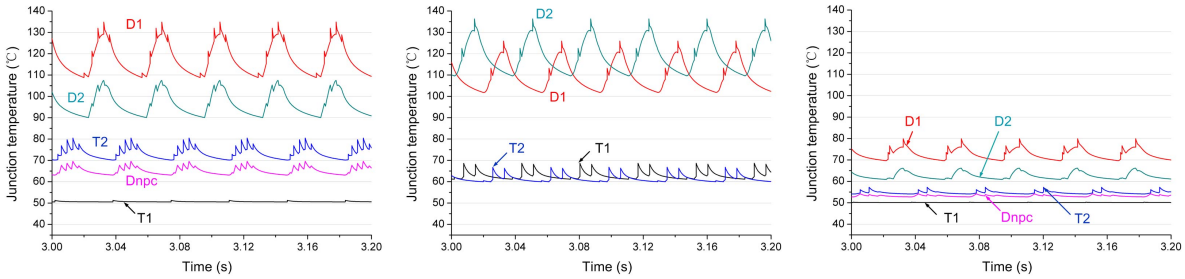

(a) 3L-NPC BTB (b) 3L-HB BTB (c) 5L-HB BTB

Fig. 14: Thermal distribution of generator side converters with direct-drive PMSG (v_w=11.7 m/s, f_e=27.5 Hz).

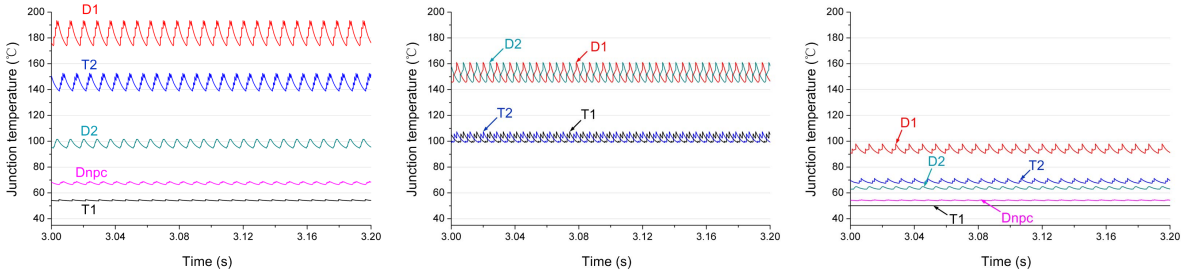

(a) 3L-NPC BTB (b) 3L-HB BTB (c) 5L-HB BTB

Fig. 15: Thermal distribution of generator side converters with one-stage gear box drive PMSG (v_w=11.7 m/s, f_e=120 Hz).

For the 3L-NPC topology, the thermal distribution is still quite unequal both with PMSG_DD and PMSG_1G, the outer freewheeling diode D1 becomes the hottest device, as shown in Fig. 14 (a) and Fig. 15 (a). The 3L-HB topology shows much worse thermal distribution equality in Fig. 14 (b) and Fig. 15 (b) compared to the grid side in Fig. 11 (b), and reaches the similar maximum junction temperature as the 3L-NPC generator side converter. For the 5L-HB topology the thermal distribution equality has no significant change compared to the grid side, and still maintains the most potential to reduce the current rating of power devices among the three generator side converter topologies.

The further comparison of junction temperature fluctuation ΔT_j and mean value T_m with relation to the wind speed v_w between different generator side converters are shown in Fig. 16 and Fig. 17 respectively, where the most extreme loaded power devices in each converter solution are indicated. The parameters for the generator side converter at different wind speeds can be found in Table VII. It can be seen that, 3L-NPC shows both the largest ΔT_j as well as T_m during the whole operation range of wind speeds in the two drive systems. Compared to the 3L-NPC topology, the 3L-HB converter no longer shows advantages of the thermal performances with PMSG_DD, as shown in Fig. 16 (a) and Fig. 17 (a), and it has limited improvements of the thermal performances with PMSG_1G, as shown in Fig. 16 (b) and Fig. 17 (b). While for the 5L-HB BTB, it still achieves significant advantages of the thermal performances compared to the 3L-NPC and 3L-HB solutions both in the direct drive and one-stage gear box drive system.

It is noted that, although all of the converter candidates with PMSG_1G have much higher loss in the power devices, they can achieve even smaller junction temperature fluctuation ΔT_j compared to the converters with PMSG_DD, as shown in Fig. 16 (b) compared to Fig. 16 (a). This is because of more frequent loss cycling (120 Hz), which will contribute to the reduction of junction temperature fluctuation. However, the junction temperature mean value T_m of each converter with PMSG_1G is

much higher than that with PMSG_DD, as shown in Fig. 17 (b) compared to Fig. 17 (a). Only 5L-HB topology can keep the maximum junction temperature below the maximum allowable temperature limitation of 125 ℃ during the whole operation range of wind speed. Therefore, 5L-HB topology seems to be the only choice as the generator side converter in the one-stage gear box drive system.

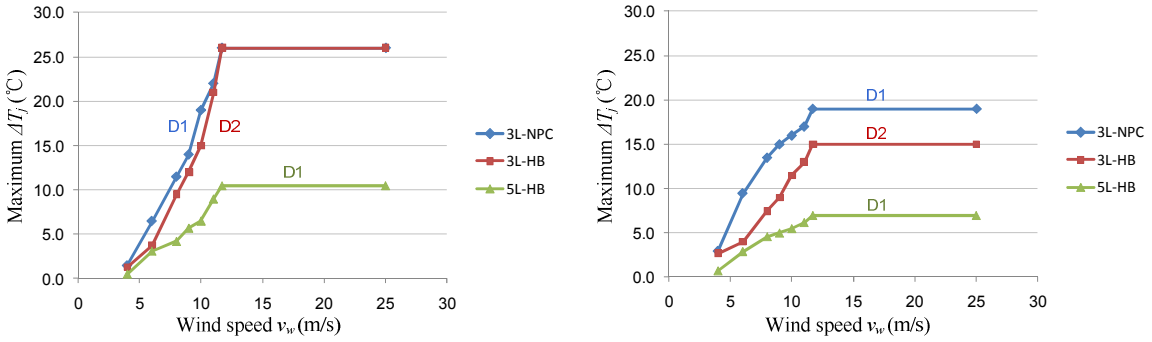

(a) Direct-drive (b) One-stage gear box drive

Fig. 16: Temperature fluctuation ΔT_j vs. wind speed v_w of generator side converters

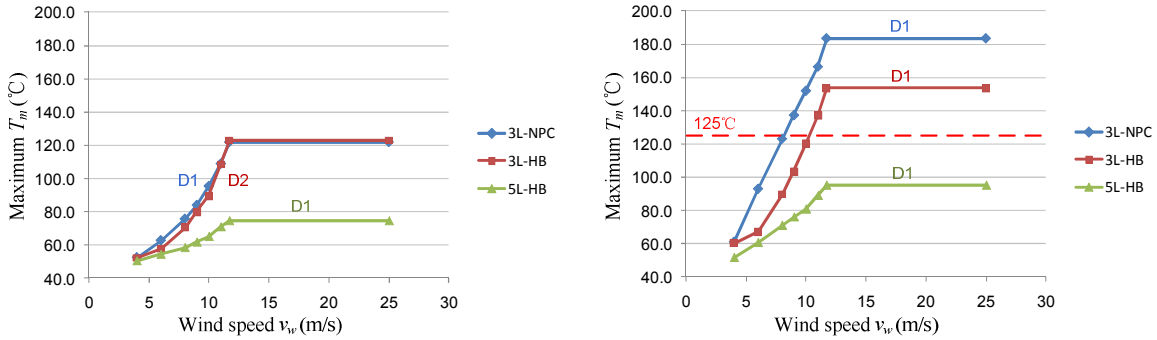

(a) Direct-drive (b) One-stage gear box drive

Fig. 17: Temperature mean value T_m vs. wind speed v_w of generator side converters

Table VII: The parameters of generator side converter (PMSG_DD/PMSG_1G)

Wind speed v_w (m/s)	**4**	**6**	**8**	**9**	**10**	**11**
Generator power P_G (MW)	0.4	1.4	3.2	4.6	6.3	8.4
Rotor speed n_r (rpm)	3.6/34.9	5.5/53.4	7.3/70.8	8.2/79.5	9.1/88.3	10.0/97.0
Induced voltage E_p (Vrms)*	675/649	1031/990	1368/1315	1537/1477	1706/1638	1874/1800
Electrical frequency f_e (Hz)	10.0/43	15.0/66	20.1/87	22.6/98	25.0/109	27.5/120
Switching frequency f_s (Hz)	275/1200					

*Phase voltage in the stator for 3L-NPC and 3L-HB, and half for 5L-HB.

Life time estimation

With the information of junction temperature fluctuation ΔT_j and mean value T_m, the number of cycles to failure of the power devices can be estimated base on the well known Coffin-Manson model [18],[19] as shown in (1), which is commonly used to estimate the life time of power semiconductors. However, the parameters A, n and k in (1) have to be determined according to the experimental accelerated stress tests, which are still not provided yet by the datasheets of the selected power devices. Therefore the life time estimation results are not included in this paper.

$$N_f = A \cdot (\Delta T_j)^{-n} \cdot e^{E_a/(k \cdot T_m)} \tag{1}$$

Conclusion

Among the four 10 MW wind power converter candidates, 3L-NPC BTB seems to be the least attractive solution because of extremely unequal thermal distribution, higher mean value and more fluctuation amplitude of junction temperature both on the grid side and generator side.
The 3L-HB BTB shows excellent thermal performances on the grid side. However, it has the similar poor thermal performances as 3L-NPC BTB on the generator side both in the direct-drive and one-stage gear box drive system.
The 5L-HB BTB shows significant advantages of thermal performances among the four converter solutions, and it could be the only choice in the one-stage gear box drive system. But the drawback is doubled number of power switching devices compared to 3L-NPC BTB. However, this solution reserves some potential to further reduce the current rating and cost of power devices.
The 3L-NPC+5L-HB seems to be a less attractive solution because the 3L-NPC generator side converter is the "weak point" of the whole converter system, and 5L-HB is not the best choice for grid side converter.
Due to much higher thermal cycling frequency, the generator side converters in the one-stage gear box drive system could have similar or even smaller junction temperature fluctuation amplitude though dissipating much higher loss than the converters in direct-drive system. This feature could contribute to the life time extension of the power devices. However, the maximum junction temperature will be much higher than the direct-drive system due to larger mean value of junction temperature.

References

[1] F. Blaabjerg, Z. Chen, S.B. Kjaer, "Power Electronics as Efficient Interface in Dispersed Power Generation Systems", *IEEE Transactions on Power Electronics*, 2004, vol. 19, no. 4, pp. 1184-1194.

[2] Z. Chen, J.M. Guerrero, F. Blaabjerg, "A Review of the State of the Art of Power Electronics for Wind Turbines," *IEEE Transactions on Power Electronics,* vol.24, no.8, pp.1859-1875, Aug. 2009.

[3] Website of Vestas Wind Power, wind turbines overview, April 2011. (Available: http://www.vestas.com/)

[4] O. S. Senturk, L. Helle, S. Munk-Nielsen, P. Rodriguez, R. Teodorescu, "Medium voltage three-level converters for the grid connection of a multi-MW wind turbine," in *Proc. EPE'09*, pp: 1- 8, 2009.

[5] M. Altin, O. Goksu, R. Teodorescu, P. Rodriguez, B. Bak-Jensen, L. Helle, "Overview of recent grid codes for wind power integration," Proc. of OPTIM'2010, pp.1152-1160, 2010.

[6] S. Kouro, M. Malinowski, K. Gopakumar, J. Pou, L. G. Franquelo, B. Wu, J. Rodriguez, M. A. Perez, J. I. Leon, "Recent Advances and Industrial Applications of Multilevel Converters," *IEEE Transactions on Power Electronics*, vol. 57, no. 8, pp. 2553 – 2580, 2010.

[7] D. Krug, S. Bernet, S. S. Fazel, K. Jalili, M. Malinowski, "Comparison of 2.3-kV Medium-Voltage Multilevel Converters for Industrial Medium-Voltage Drives," *IEEE Transactions on Industrial Electronics,* vol. 54, no. 6, pp. 2979-2992, 2007.

[8] J. Rodriguez, S. Bernet, P. K. Steimer, I. E. Lizama, "A Survey on Neutral-Point-Clamped Inverters," *IEEE Transactions on Industrial Electronics,* vol. 57, no. 7, pp. 2219-2230, 2010.

[9] T. Bruckner, S. Bernet, H. Guldner, "The active NPC converter and its loss-balancing control," *IEEE Transactions on Industrial Electronics,* vol. 52, no. 3, pp.855-868, 2005.

[10] J. Holtz, N. Oikonomou, "Optimal Control of a Dual Three-Level Inverter System for Medium-Voltage Drives," *IEEE Transactions on Industrial Applications,* vol. 46, no. 3, pp. 1034-1041, 2010.

[11] H. Hosoda, S. Peak, "Multi-level converters for large capacity motor drive," in *Proc. IECON'10*, pp. 516-522, 2010.

[12] H. Li, Z. Chen, H. Polinder, "Optimization of Multibrid Permanent-Magnet Wind Generator Systems," *IEEE Transactions on Energy Conversion,* vol. 24, no. 1, pp. 82-92, 2009.

[13] H.Polinder, F.F.A.van der Pijl, G.-J.de Vilder, P.J.Tavner, "Comparison of direct-drive and geared generator concepts for wind turbines," *IEEE Transactions on Energy Conversion,* vol. 21, no. 3, pp. 725-733, 2006.

[14] F. Blaabjerg, U. Jaeger, S. Munk-Nielsen and J. Pedersen, "Power Losses in PWM-VSI Inverter Using NPT or PT IGBT Devices," *IEEE Transactions on Power Electronics,* vol. 10, no. 3, pp. 358–367, May 1995.

[15] ABB Application Note: Applying IGBTs, May 2007.

[16] User manual of PLECS blockset version 3.1, March 2011. (Available: http://www.plexim.com/files/plecsmanual.pdf).

[17] O. Apeldoorn, B. Odegard, P. Steimer, S. Bernet, "A 16 MVA ANPC-PEBB with 6 kA IGCTs," in *Proc. IAS'05*, vol.2, pp. 818-824, 2005.

[18] W. Lixiang, J. McGuire,R.A. Lukaszewski, "Analysis of PWM Frequency Control to Improve the Lifetime of PWM Inverter," *IEEE Transactions on Industrial Electronics,* vol. 47, no. 2, pp. 922-929, 2011.

[19] I.F. Kovac□evi□, U. Drofenik, J.W. Kolar, "New physical model for lifetime estimation of power modules," in *Proc. IPEC'10*, pp. 2106-2114, 2010.